Front. Phys. 12(5), 124502 (2017)
DOI 10.1007/s11467-017-0689-3

RESEARCH ARTICLE

# Extended social force model with a dynamic navigation field for bidirectional pedestrian flow

**Yan-Qun Jiang[1,*,†], Bo-Kui Chen[2,*,‡], Bing-Hong Wang[3,*,§], Weng-Fai Wong[2], Bing-Yang Cao[4]**

[1] *School of Science, Southwest University of Science and Technology, Mianyang 621000, China*
[2] *School of Computing, National University of Singapore, Singapore 117417, Singapore*
[3] *Department of Modern Physics and Nonlinear Science Center, University of Science and Technology of China, Hefei 230026, China*
[4] *Key Laboratory for Thermal Science and Power Engineering of Ministry of Education, Department of Engineering Mechanics, Tsinghua University, Beijing 100084, China*
*Corresponding authors. E-mail:* [†] *jyq2005@mail.ustc.edu.cn,* [‡] *chenssx@mail.ustc.edu.cn,* [§] *bhwang@ustc.edu.cn*
*Received January 25, 2017; accepted April 14, 2017*

An extended social force model with a dynamic navigation field is proposed to study bidirectional pedestrian movement. The dynamic navigation field is introduced to describe the desired direction of pedestrian motion resulting from the decision-making processes of pedestrians. The macroscopic fundamental diagrams obtained using the extended model are validated against camera-based observations. Numerical results show that this extended model can reproduce collective phenomena in pedestrian traffic, such as dynamic multilane flow and stable separate-lane flow. Pedestrians' path choice behavior significantly affects the probability of congestion and the number of self-organized lanes.

**Keywords** bidirectional pedestrian flow, social force model, dynamic navigation field, collective phenomena, complex systems

**PACS numbers** 45.70.-n, 05.65.+b, 89.75.k



## 1 Introduction

Pedestrian movement is an important factor in the design and optimization of transportation facilities, pedestrian walkways, and public transport intersections. Further, complex situations involving bidirectional pedestrian movement occur continually when enormous numbers of people with different final destinations use pedestrian facilities, such as crosswalks, sidewalks, corridors, and stairways. Therefore, problems related to bidirectional pedestrian flow and its effects on pedestrian dynamics have attracted considerable attention from scientists and engineers in recent decades [1–7].

Many behavioral investigations and empirical studies [3, 7–12] have been conducted to gain a good understanding of bidirectional pedestrian flow characteristics. Many phenomena such as self-organization and synchronization have been observed in pedestrian flow [8, 13, 14]. Synchronization has also been studied in other fields [15, 16]. Empirical observations are preferable for analyzing qualitative self-organization phenomena, such as the formation of lanes and the occurrence of congestion at sufficiently high densities, and obtaining fundamental diagrams. The fundamental diagrams representing the relationships among density, velocity, and flow generally differ for various walking facilities [10, 11]. They can quantify the capacity of pedestrian facilities and support the construction of reliable pedestrian simulation models [3, 5, 17, 18]. A number of simulation models for pedestrian dynamics, including hydrodynamic models [4, 19–23], mesoscopic (kinetic) models [24, 25], the social force model [1, 26–30], the cellular automaton model [2, 31, 32], and the lattice gas model [33, 34], have been proposed recently to simulate and reproduce collective behaviors appearing in bidirectional pedestrian movement. Examples of collective patterns caused by local interactions among conflicting pedestrians are jamming, lane formation, and oscillations at narrow bottlenecks in bidirectional pedestrian streams [28, 33, 35]. Optimal self-organized phenomena such as the spontaneous formation of lanes of uniform walking direction can help to reduce conflicts with pedestrians moving in the op-

*These authors contributed equally to this work.
arXiv: 1705.03569.

posite direction and increase the efficiency of walking [8, 13].

Most simulation models of bidirectional pedestrian flow can describe the basic behavioral characteristics qualitatively [1, 2, 4, 19–22, 27, 28, 31–34]. In this work, we consider only the social force model owing to its many advantages. For example, it captures the mutual influence of individual pedestrians in a two-dimensional (2D) continuous space by defining social analogs of physical forces, e.g., repulsive interactions, frictional forces, dissipation, and fluctuations [1]. In this way, the detailed behavior of individual pedestrians can be considered, which makes the simulated pedestrians more realistic [27]. The social force model first proposed by Helbing and Molnár [1] has been modified in numerous ways [6, 28, 36–40]. For instance, Guo [28] introduced spatial and temporal separation rules to reproduce self-organizing movement patterns of pedestrians, e.g., oscillatory flow and three classes of lane formation: unidirectional, mixed, and separate. Kretz *et al.* introduced the notion of the "quickest path" using a non-iterative method to describe the path choice behavior of pedestrians [39]. Karamouzas *et al.* used a novel statistical–mechanical approach to describe human interactions across a wide variety of situations, speeds, and densities [40]. However, in the social force model, where pedestrians choose their paths by a shortest-distance strategy, the decision-making process of pedestrians walking in a dynamic environment is tactically simplified. Path choice strategy is not only a research field in pedestrian flow, but also a hot topic in traffic flow, and many research results have been reported [41–47].

In this paper, we revise Helbing's model by introducing a reactive user-equilibrium path choice strategy to simulate bidirectional pedestrian flow and analyze the effect of path choice behaviors on bidirectional pedestrian movement. This path choice strategy, which determines a continuous dynamic navigation field, i.e., the desired walking direction of individual pedestrians, has been used in some hydrodynamic models [19, 20, 22], in which pedestrians in a group, acting as a "thinking" crowd flow, are assumed to choose a path with the lowest instantaneous walking cost on the basis of the instantaneous traffic information available to them when they make their decisions. These hydrodynamic models can describe well the global properties of the pedestrians but cannot describe in detail the behavioral characteristics of individual pedestrians, such as their static and dynamic obstacle avoidance behaviors. The paper is structured as follows. The extended social force model of bidirectional pedestrian traffic and its numerical method are described in Section 2. Numerical simulation results are presented in Section 3. Finally, Section 4 summarizes the results and presents concluding remarks.

## 2 Dynamic pedestrian model

The well-known social force model [1] is a microscopic, force-based model in which all pedestrians are treated as self-driven particles, and their behaviors are described by a mixture of socio-psychological and physical forces. This model is developed to simulate two groups of pedestrians, Group 1 and Group 2, walking in a 2D continuous walking facility denoted as $\Omega$. The pedestrians in each group have the same travel destination, e.g., one of the two exits of the walking facility. For instance, each pedestrian in Group $k$ ($k \in \{1, 2\}$), who has mass $m_i^k$ and radius $r_i^k$ and is located at the position $\boldsymbol{r}_i^k(t) \in \Omega$, prefers to move with a certain desired speed $v_d^k$ in a certain direction $\boldsymbol{e}_i^k(t)$, and thus tends to adapt his or her actual velocity $\boldsymbol{v}_i^k(t)$ accordingly with a certain characteristic time $\tau_i^k$. Simultaneously, pedestrian $i$ in Group $k$ will try to maintain a distance from another pedestrian $j$ in the two groups and from the walls $w$ according to the interaction forces $\boldsymbol{f}_{ij}^k$ and $\boldsymbol{f}_{iw}^k$, respectively. To take into account the effect of perception, we define the sensory field $R_i^k$ for pedestrian $i$ in Group $k$ as

$$R_i^k = \{\boldsymbol{r} \in \Omega : (\boldsymbol{r} - \boldsymbol{r}_i^k) \cdot \boldsymbol{e}_i^k > 0, |\boldsymbol{r} - \boldsymbol{r}_i^k| \le R_0\}, \quad (1)$$

where $R_0$ represents the sensory range of pedestrians. The sensory field $R_i^k$ is usually anisotropic and short-range, which means that pedestrian $i$ in Group $k$ can interact only with pedestrians who are within his/her sensory field.

### 2.1 Model description

The movement of individual pedestrians in Group $k$ can be described by nonlinear ordinary differential equations (ODEs) according to Newton's law:

$$\frac{\mathrm{d}\boldsymbol{r}_i^k}{\mathrm{d}t} = \min(v_{\max}, \|\boldsymbol{v}_i^k\|)\frac{\boldsymbol{v}_i^k}{\|\boldsymbol{v}_i^k\|}, \quad (2)$$

$$\frac{\mathrm{d}\boldsymbol{v}_i^k}{\mathrm{d}t} = \frac{v_d^k \boldsymbol{e}_i^k - \boldsymbol{v}_i^k}{\tau_i^k} + \frac{\sum_{j\neq i} \boldsymbol{f}_{ij}^k + \sum_w \boldsymbol{f}_{iw}^k}{m_i^k}. \quad (3)$$

Here, the change in position $\boldsymbol{r}_i^k(t)$ is given by the velocity $\boldsymbol{v}_i^k(t)$ of pedestrian $i$ in Group $k$, and $v_{\max}$ is the maximal acceptable speed of pedestrians.

In Eq. (3), the first force, $(v_d^k \boldsymbol{e}_i^k - \boldsymbol{v}_i^k)/\tau_i^k$, is an attractive force that drives pedestrian $i$ in Group $k$ to move toward his/her goal. The interaction force $\boldsymbol{f}_{ij}^k$ includes the social force $\boldsymbol{F}_{ij}^k$ and the granular force $\boldsymbol{G}_{ij}^k$; i.e., $\boldsymbol{f}_{ij}^k = \boldsymbol{F}_{ij}^k + \boldsymbol{G}_{ij}^k$. Here, the social force $\boldsymbol{F}_{ij}^k$ is defined as

$$\boldsymbol{F}_{ij}^k = A\exp[(r_{ij} - d_{ij})/B]\cos(\theta_{ij})\boldsymbol{n}_{ij}, \quad j \in M_i, \quad (4)$$

where $A$ and $B$ are constants that determine the strength and range of the interaction, respectively; $r_{ij}$ is the sum

of the radii of pedestrians $i$ and $j$; $d_{ij}$ denotes the distance between pedestrians $i$ and $j$; $\boldsymbol{n}_{ij}$ is the unit vector pointing from pedestrian $j$ to pedestrian $i$; $\theta_{ij}$ is the angle between $\boldsymbol{e}_i^k$ and $-\boldsymbol{n}_{ij}$; and $M_i$ is the set of all pedestrians in the sensory region $R_i^k$. The granular force $\boldsymbol{G}_{ij}^k$ is described as

$$\boldsymbol{G}_{ij}^k = -\varepsilon_{ij}\gamma\boldsymbol{n}_{ij} - \varepsilon_{ij}\kappa\Delta v_{ji}^t\boldsymbol{t}_{ij} + \eta\Delta v_{ji}^n\boldsymbol{n}_{ij}, \quad j \in N_i, \tag{5}$$

where $\varepsilon_{ij} = r_{ij} - d_{ij}$; $\gamma$, $\kappa$, and $\eta$ determine obstruction effects in physical interactions; $\Delta v_{ji}^t$ and $\Delta v_{ji}^n$ are the tangential and normal velocity differences, respectively; $\boldsymbol{t}_{ij}$ is the tangential unit vector, which is orthogonal to $\boldsymbol{n}_{ij}$; and $N_i$ is the set of all pedestrians who have any physical contact with pedestrian $i$ in Group $k$, i.e., $\varepsilon_{ij} \leq 0$. In Eq. (5), the term $\eta\Delta v_{ji}^n\boldsymbol{n}_{ij}$ represents a physical damping force with the damping parameter $\eta$ [36].

The interaction force $\boldsymbol{f}_{iw}^k$ generated by the interaction between pedestrian $i$ in Group $k$ and the nearest wall $w$ such that the pedestrian avoids the wall before touching it is described in a form analogous to that of the two-body interaction $\boldsymbol{f}_{ij}^k$.

### 2.2 Definition of the dynamic navigation field

We assume that all pedestrians in Group $k$ are familiar with the surroundings, e.g., the locations of walls and exits, and know the current traffic conditions that obtain when they make decisions. They prefer to walk in a reactive user-optimal manner to minimize their total instantaneous cost from location $\boldsymbol{r}$ to the final destination, e.g., one of the two exits of the walking facility. For Group $k$, the minimum total instantaneous walking cost is denoted as $\Phi^k(\boldsymbol{r})$, and $\Phi^k(\boldsymbol{r}) = 0$ at the exit represented by $\Gamma^k$.

We denote the local travel cost at location $\boldsymbol{r}$ as $C^k(\boldsymbol{r})$; it represents the walking cost per unit distance of movement incurred by pedestrians in Group $k$ and is defined as

$$C^k(\boldsymbol{r}) = \frac{1}{v_d^k} + \omega_1[1-\cos(\Psi)][\rho^{l(\neq k)}(\boldsymbol{r})]^2 + \omega_2[\rho^1(\boldsymbol{r}) + \rho^2(\boldsymbol{r})]^2. \tag{6}$$

Here, $l \in \{1, 2\}$; $\omega_1$ and $\omega_2$ are weight coefficients; $\Psi$ is the angle between the vectors $\boldsymbol{e}^1(\boldsymbol{r})$ and $\boldsymbol{e}^2(\boldsymbol{r})$, where $\boldsymbol{e}^k(\boldsymbol{r})$ is the desired direction of motion for Group $k$ at location $\boldsymbol{r}$; and $\rho^k(\boldsymbol{r})$ is the local density of Group $k$ at location $\boldsymbol{r}$. In Eq. (6), the term $1/v_d^k$, which is the major factor, represents the cost associated with the travel time, and the terms $\omega_1[1-\cos(\Psi)][\rho^{l(\neq k)}(\boldsymbol{r})]^2$ and $\omega_2[\rho(\boldsymbol{r})]^2$, which are the minor factors, represent other associated costs such as a preference for reducing collision conflicts with pedestrians in the other group and avoiding high-density regions to feel comfortable, respectively. For Group $k$, the local density $\rho^k(\boldsymbol{r})$, which is used to evaluate the crowdedness level within the subarea at location $\boldsymbol{r}(t)$, is measured as

$$\rho^k(\boldsymbol{r}) = \sum_i f(\|\boldsymbol{r}_i^k - \boldsymbol{r}\|), \tag{7}$$

where

$$f(z) = \frac{\exp(\frac{-z^2}{2R^2})}{2\pi R^2} \tag{8}$$

with a measurement parameter $R = 0.7$ m.

The minimum total instantaneous walking cost $\Phi^k(\boldsymbol{r})$ incurred by pedestrians in Group $k$ from the origin $\boldsymbol{r}$ to the destination $\Gamma^k$ is calculated as

$$\Phi^k(\boldsymbol{r}) = \Phi^k(\boldsymbol{r}_d) + \min_p \int_p C^k(\boldsymbol{r})\mathrm{d}s, \tag{9}$$

where $\boldsymbol{r}_d \in \Gamma^k$, and $p$ denotes any path from the origin $\boldsymbol{r}$ to the destination $\Gamma^k$. According to [20], the rate of reduction in the cost potential $\Phi^k(\boldsymbol{r})$ for Group $k$ is greatest along the direction of motion. Thus, the desired direction of motion for Group $k$ at location $\boldsymbol{r}$ is obtained as [20, 22]

$$\boldsymbol{e}^k(\boldsymbol{r}) = -\frac{\nabla\Phi^k(\boldsymbol{r})}{\|\nabla\Phi^k(\boldsymbol{r})\|}, \tag{10}$$

which determines a dynamic navigation field for bidirectional pedestrian movement in the 2D continuous domain $\Omega$.

Furthermore, the cost potential for Group $k$ satisfies the following Eikonal equation [20]:

$$\begin{aligned} &\|\nabla\Phi^k(\boldsymbol{r})\| = C^k(\boldsymbol{r}), \quad \boldsymbol{r} \in \Omega, \\ &\Phi^k(\boldsymbol{r}) = 0, \quad \boldsymbol{r} \in \Gamma^k. \end{aligned} \tag{11}$$

The extended social force model described in Section 2 is solved as follows:

Step 1. Given the location and speed of pedestrian $i$ in Group $k$, $\boldsymbol{r}_i^{k,n}$ and $\boldsymbol{v}_i^{k,n}$, respectively, at time $t^n$ $(n = 0, 1, 2, \ldots)$, estimate the local density $\rho^k(\boldsymbol{r})$ using Eq. (7), and then solve Eq. (11) by a fast sweeping method [20, 48] to determine the dynamic navigation field for bidirectional pedestrian flow. The desired walking direction of pedestrian $i$ in Eq. (3) is obtained using Eq. (10).

Step 2. Solve the system of first-order ODEs composed of Eqs. (2) and (3) by the second-order Runge–Kutta method and then update its solution as $\boldsymbol{r}_i^{k,n+1}$ and $\boldsymbol{v}_i^{k,n+1}$ at time $t^{n+1} = t^n + \Delta t$.

Step 3. Stop the calculation process if all pedestrians leave the walking facility. Otherwise, replace $n$ with $n+1$ and go to Step 1.

Here, $\Delta t$ is the size of the time step in the simulation.

## 3 Numerical simulations

Several parameters in our model are set as follows: for each pedestrian in Group $k$, $r_i^k = 0.25$ m, $m_i^k = 80$ kg, $\tau_i^k = 0.5$ s, $A = 2000$ N, $B = 0.08$ m, $k = 1.2\times10^5$ kg/s$^2$, $\kappa = 2.4 \times 10^5$ kg/(m·s), and $\eta = 100$ kg/s [26, 36]. The sensory radius in Eq. (1) is $R_0 = 3$ m. In Eq. (2), the desired walking speed is $v_d^k = 1.034$ m/s [7], and the maximum walking speed is $v_{\max} = 1.3v_f$. In Eq. (6), $\omega_2 = 0.05$. The size of the time step in the simulation, $\Delta t$, is set to 0.01 s.

To calibrate and test the extended model, we used experimental data from a series of controlled experiments of bidirectional pedestrian streams collected by Wong *et al.* [7]. The macroscopic fundamental diagrams of bidirectional pedestrian flow were validated against camera-based observations. Numerical simulations of bidirectional pedestrian movement were performed in a 14-m-long and 3-m-wide corridor. Each pedestrian stream entered this corridor from one of the two ends of the corridor. The dimensions and configuration of the region of interest (ROI) are shown in Fig. 1. Let $\rho^c$ and $v^c$ be the average density and speed of the reference stream, respectively. Here, the average density $\rho^c$ (in ped/m$^2$) and the average speed $v^c$ (in m/s) in the ROI are computed as the number of reference people in the ROI divided by the area of the ROI and the sum of their walking speeds divided by the area of the ROI, respectively. The specific flow of the reference stream is expressed as $J^c$ [in ped/(m·s)], which is equal to $\rho^c \times v^c$.

Figure 2 compares the fundamental diagrams of bidirectional pedestrian flow for the camera-based observations and simulation results obtained with different values of the weight coefficient $\omega_1$. There are no extra collision conflicts between the two streams at $\omega_1 = 0$. At larger $\omega_1$ values, pedestrians have a more obvious tendency to reduce collision conflicts with other pedestrians in the conflicting stream. Figure 2 shows that the fundamental diagrams for the simulation data obtained with various values of $\omega_1$ agree well with those for the observations, and no large differences are found in the observed density range, $\rho^c < 2$ ped/m$^2$. The specific flow $J^c$ increases as the density $\rho^c$ increases from 0 to 2 ped/m$^2$, which implies that the reference stream is in an uncongested state. Differences in the fundamental diagrams for the simulation data can be observed for densities $\rho^c > 2$ ped/m$^2$. From Fig. 2(a), the specific

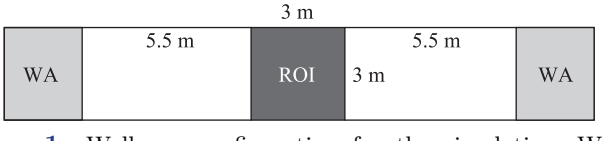


**Fig. 1** Walkway configuration for the simulation. WA: Waiting area; ROI: Region of interest.

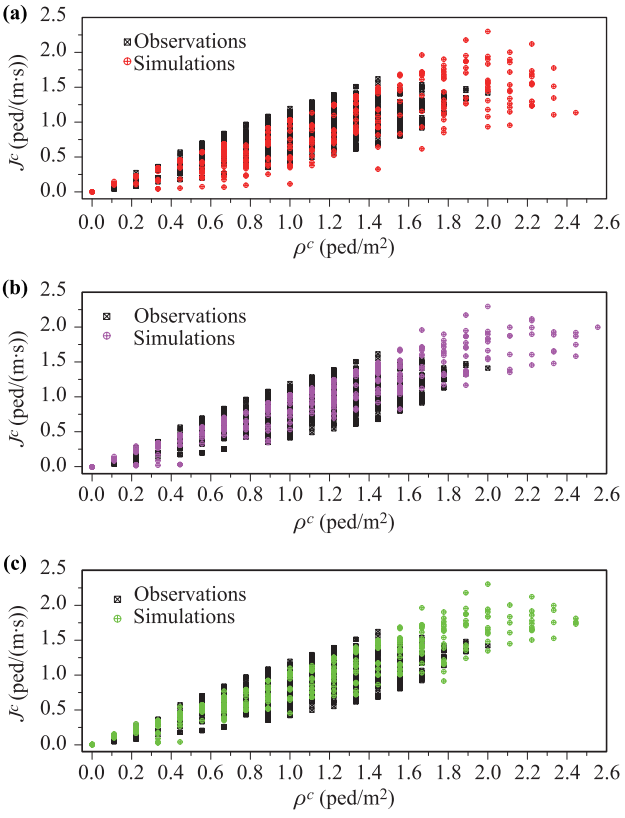


**Fig. 2** Comparisons of fundamental diagrams of observations and simulation data. **(a)** $\omega_1 = 0$; **(b)** $\omega_1 = 0.1$; **(c)** $\omega_1 = 0.2$.

flow $J^c$ for $\omega_1 = 0$ clearly decreases as the density $\rho^c$ increases beyond 2 ped/m$^2$, which indicates that the reference stream is in a congested state. Therefore, the critical density at which the maximum flow is achieved is about 2 ped/m$^2$ for $\omega_1 = 0$. The critical density for $\omega_1 > 0$ is slightly larger than that for $\omega_1 = 0$, indicating that the probability of congestion will decrease at a larger value of $\omega_1$ under the same conditions. The credibility of the data produced by the extended model can be validated by comparing them with the findings from the controlled experiments of bidirectional pedestrian streams.

Figure 3 compares the fundamental diagrams of bidi-

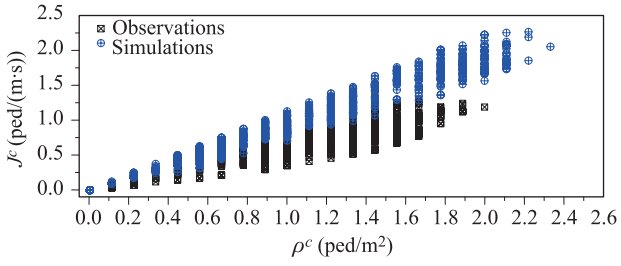


**Fig. 3** Comparisons of fundamental diagrams of observations and simulation data obtained using Helbing's model.

rectional pedestrian flow for the camera-based observations and the simulation results obtained by Helbing's model. In this model, the desired walking directions for the two streams are set to $(1, 0)$ and $(-1, 0)$, respectively. The specific flow $J^c$ based on the previous experimental results is found to be significantly larger than that based on Helbing's model, especially at relatively high density (i.e., $\rho^c > 0.7$ ped/m$^2$). Thus, the setting of the desired directions in Helbing's model, which describes the shortest-path strategy of pedestrians, is inappropriate at relatively high density. In contrast, Fig. 2 shows that the reactive user-equilibrium path choice strategy introduced in the extended model is rather appropriate in this case.

Using open boundary conditions, we conduct numerical simulations of bidirectional pedestrian movement in a 40 m×10 m corridor. Initially, the corridor is empty. Pedestrians enter the corridor from both ends at random. The inflow value for each group is set to 6 ped/s during a simulation that lasts 600 s, and the inflow pattern is similar for all simulations. Note that 600 s for each simulation is long enough for the bidirectional flow study because the length of the corridor in our simulation is only 40 m, and a pedestrian requires only about 40 s to traverse the corridor.

Figure 4 shows snapshots of the simulation process obtained with the weight coefficient $\omega_1 = 0$. The black squares represent pedestrians walking toward the right exit of the corridor, and the red balls represent pedestrians walking toward the left exit. We can see clearly that the opposing flows are mixed, and unstable lanes

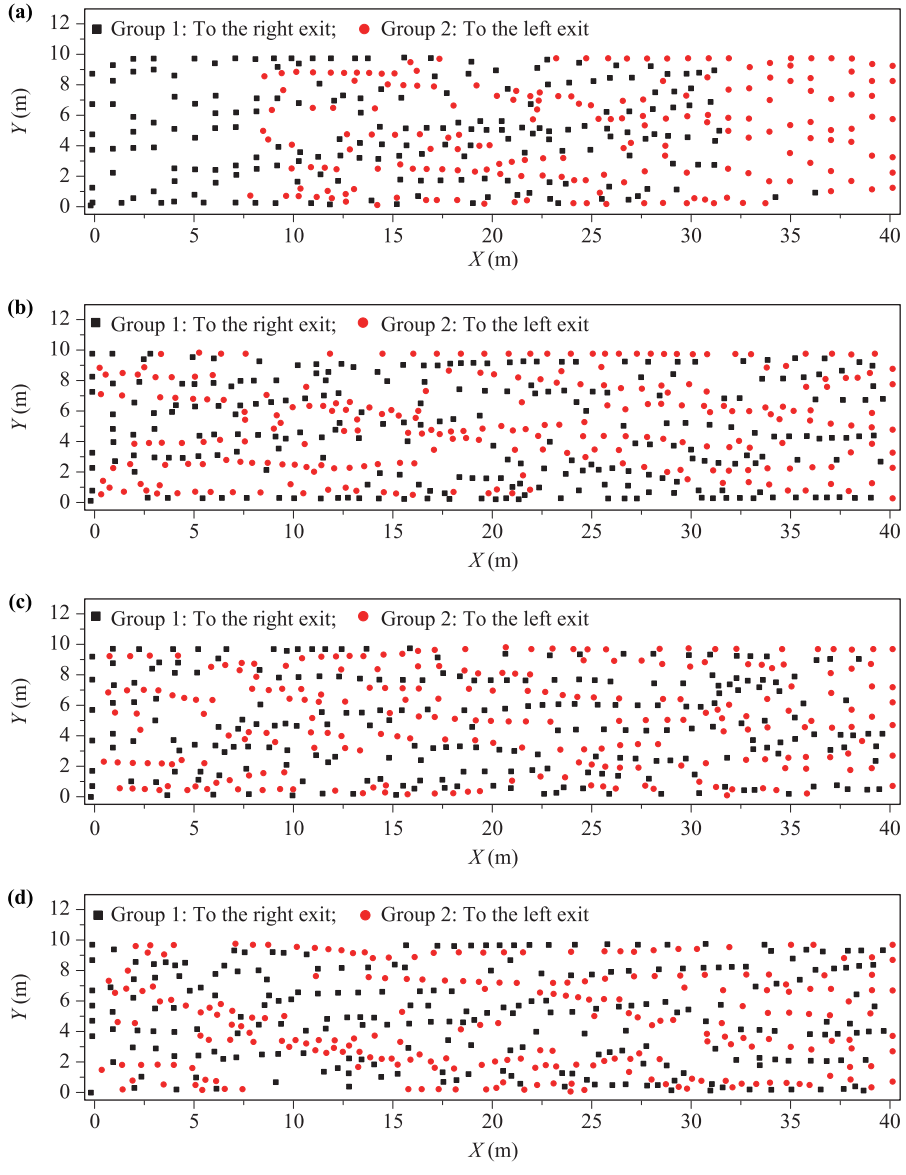


**Fig. 4** Spatial distribution of pedestrians obtained with $\omega_1 = 0$. **(a)** $t = 30$ s; **(b)** $t = 40$ s; **(c)** $t = 240$ s; **(d)** $t = 480$ s.

consisting of pedestrians who intend to walk in the same direction are formed. The lanes vary in time and space. This regime is the dynamic multilane (DML) regime observed in controlled experiments of bidirectional pedestrian movement [10].

Figure 5 shows snapshots of the simulation process obtained with $\omega_1 = 0.1$. We observe complete segregation of the two opposing streams as a result of the two groups of pedestrians' strong collision avoidance behavior. This self-organized pattern of motion enhances the pedestrian flow by reducing the collision probability. Three separate lanes are clearly formed autonomously immediately after the simulation begins and remain stable during the simulation process. This regime is called stable separate lanes (SSL) regime [10].

SSL flows are also observed for $\omega_1 = 0.2$ (Fig. 6). From Fig. 6, the opposing streams segregate themselves and occupy identical shares of the corridor, as if there is a partition line in the corridor; i.e., a quasi-symmetric spatial distribution is formed. The number of self-organized lanes decreases, as pedestrians have a more obvious tendency to reduce collision conflicts with other pedestrians in the conflicting stream. It is observed that the optimal path choice strategy of pedestrians can cause different spatial distributions of pedestrians in the corridor according to the value of the weight coefficient $\omega_1$.

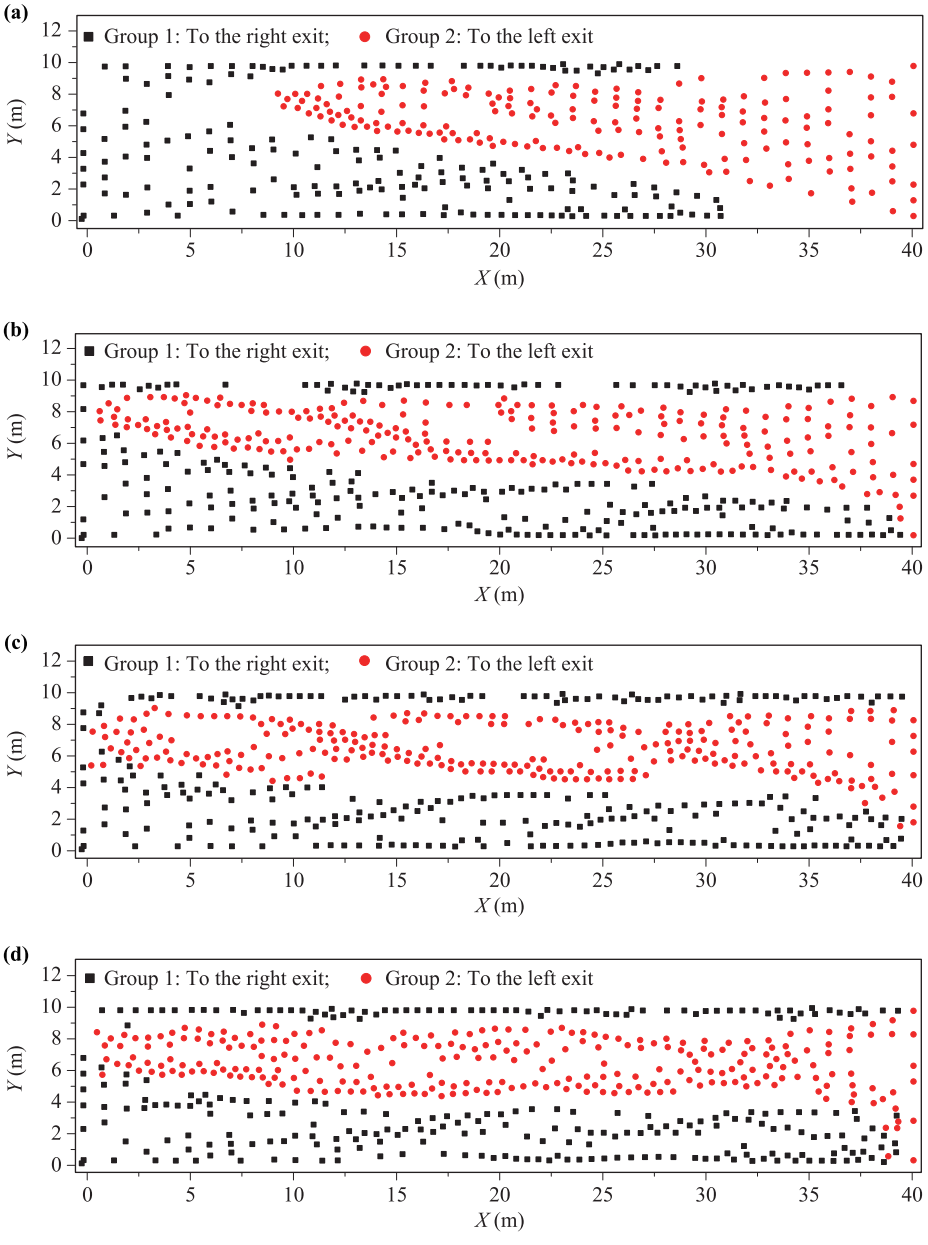


**Fig. 5** Spatial distribution of pedestrians obtained with $\omega_1 = 0.1$. **(a)** $t = 30$ s; **(b)** $t = 40$ s; **(c)** $t = 240$ s; **(d)** $t = 480$ s.

Figure 7 plots the dynamic navigation fields obtained for $\omega_1 = 0$, 0.1, and 0.2 at time $t = 480$ s. The dynamic navigation fields describe the desired directions of two groups of pedestrians and direct pedestrians to move toward the exits of the corridor. The navigation fields are time-varying according to the instantaneous pedestrian distribution in the corridor. They are generated by the optimal path choice strategy of pedestrians who intend to choose a path with the lowest instantaneous walking cost. This figure shows that the probability of face-to-face collisions between two pedestrians in bidirectional pedestrian flow is significantly reduced as $\omega_1$

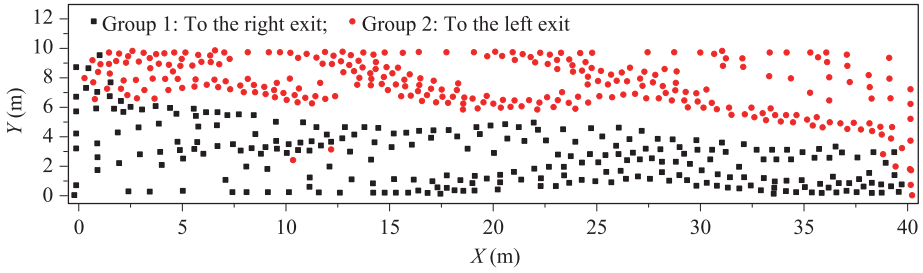


**Fig. 6** Spatial distribution of pedestrians obtained with $\omega_1 = 0.2$ at $t = 480$ s.

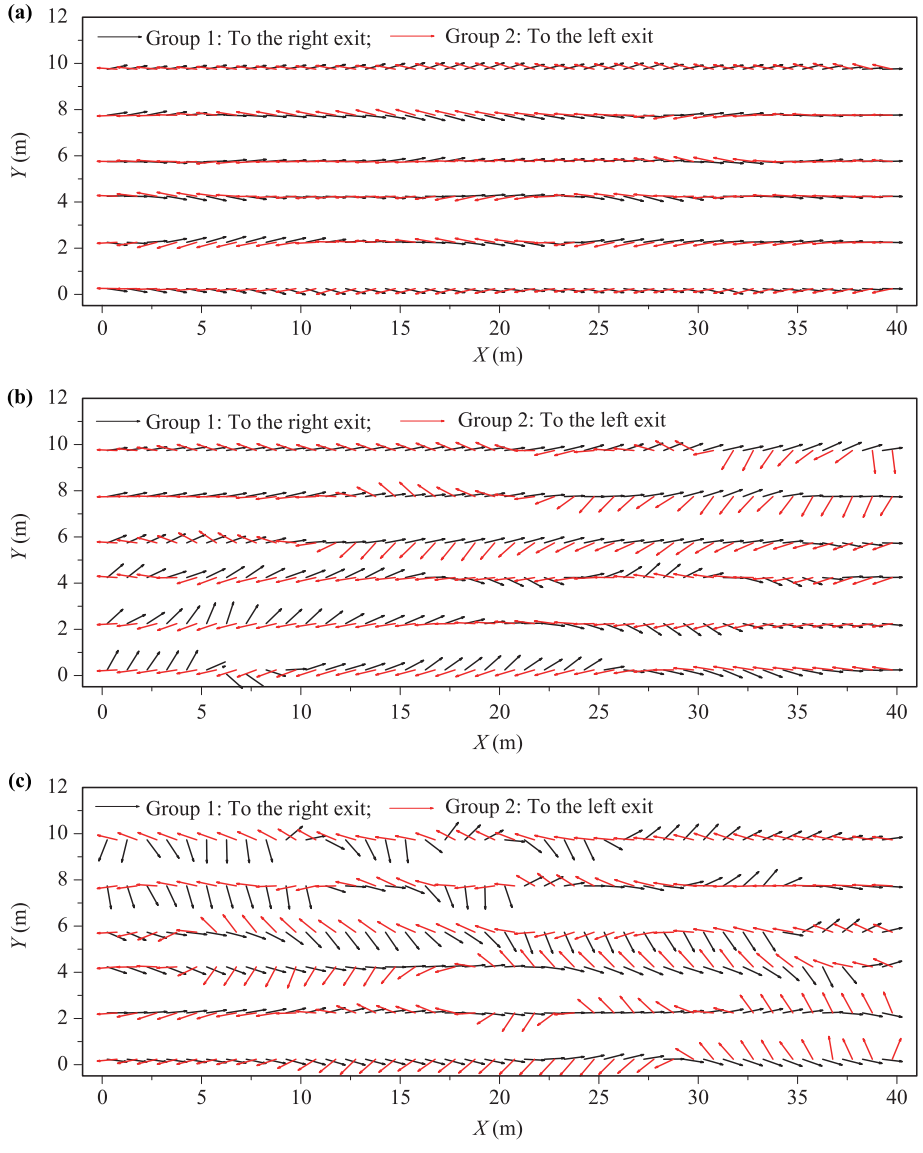


**Fig. 7** Dynamic navigation fields at $t = 480$ s. **(a)** $\omega_1 = 0$; **(b)** $\omega_2 = 0.1$; **(c)** $\omega_1 = 0.2$.

increases. This path choice strategy also produces various self-organized patterns of bidirectional pedestrian movement (Figs. 4–6).

## 4 Conclusion

Bidirectional pedestrian motion is studied using an extended social force model with a dynamic navigation field. The dynamic navigation field, which arises from the decision-making processes of pedestrians, is introduced to describe the desired direction of bidirectional pedestrian motion. Here, the desired walking direction of each group is described so as to minimize the total instantaneous cost in a reactive user-optimal manner and to reduce collision conflicts with other pedestrians in the conflicting group. The extended model of bidirectional pedestrian flow is calibrated by comparing empirical observations from controlled experiments and simulation data obtained using the simulation model. Numerical results show that pedestrians' path choice behavior significantly affects the self-organized patterns of bidirectional pedestrian movement, e.g., the DML and SSL patterns. The probability of congestion generally decreases with increasing tendency to reduce collision conflicts. Further, the number of self-organized lanes also decreases as the tendency to reduce collision conflicts increases.

**Acknowledgements** This work was supported by the National Natural Science Foundation of China (Grant Nos. 11202175, 11275186, 91024026, and FOM2014OF001), the Research Foundation of Southwest University of Science and Technology (No. 10zx7137), and a Singapore Ministry of Education Research Grant (Grant No. MOE 2013-T2-2-033).

## References

1. D. Helbing and P. Molnár, Social force model for pedestrian dynamics, *Phys. Rev. E* 51(5), 4282 (1995)
2. V. J. Blue and J. L. Adler, Cellular automata microsimulation for modeling bi-directional pedestrian walkways, *Trans. Res. Part B* 35(3), 293 (2001)
3. W. H. K. Lam, J. Y. S. Lee, and C. Y. Cheung, A study of the bidirectional pedestrian flow characteristics at Hong Kong signalized crosswalk facilities, *Transpor.* 29(2), 169 (2002)
4. R. L. Hughes, A continuum theory for the flow of pedestrians, *Trans. Res. Part B* 36(6), 507 (2002)
5. M. Isobe, T. Adachi, and T. Nagatani, Experiment and simulation of pedestrian counter flow, *Physica A* 336(3–4), 638 (2004)
6. T. I. Lakoba, D. J. Kaup, and N. M. Finkelstein, Modifications of the Helbing–Molnár–Farkas–Vicsek social force model for pedestrian evolution, *Simulation* 81(5), 339 (2005)
7. S. C. Wong, W. L. Leung, S. H. Chan, W. H. K. Lam, N. H. C. Yung, C. Y. Liu, and P. Zhang, Bidirectional pedestrian stream model with oblique intersecting angle, *J. Transp. Eng.* 136(3), 234 (2010)
8. D. Helbing, L. Buzna, A. Johansson, and T. Werner, Self-organized pedestrian crowd dynamics: Experiments, simulations, and design solutions, *Transport. Sci.* 39(1), 1 (2005)
9. T. Kretz, A. Grunebohm, M. Kaufman, F. Mazur, and M. Schreckenberg, Experimental study of pedestrian counter flow in a corridor, *J. Stat. Mech.* 2006(10), P10001 (2006)
10. J. Zhang, W. Klingsch, A. Schadschneider, and A. Seyfried, Ordering in bidirectional pedestrian flows and its influence on the fundamental diagram, *J. Stat. Mech.* P02002 (2012)
11. J. Zhang and A. Seyfried, Comparison of intersecting pedestrian flows based on experiments, *Physica A* 405, 316 (2014)
12. M. Saberi, K. Aghabayk, and A. Sobhani, Spatial fluctuations of pedestrian velocities in bidirectional streams: exploring the effects of self-organization, *Physica A* 434, 120 (2015)
13. D. Helbing and T. Vicsek, Optimal self-organization, *New J. Phys.* 13, 1 (1999)
14. T. Morbiato, R. Vitaliani, and A. Saetta, Numerical analysis of a synchronization phenomenon: Pedestrian-structure interaction, *Computers & Structures* 89(17–18), 1649 (2011)
15. C. Q. Wang, A. Pumir, N. B. Garnier, and Z. H. Liu, Explosive synchronization enhances selectivity: Example of the cochlea, *Front. Phys.* 12(5), 128901 (2017)
16. S. F. Ma, H. J. Bi, Y. Zou, Z. H. Liu, and S. G. Guan, Shuttle-run synchronization in mobile ad hoc networks, *Front. Phys.* 10(3), 100505 (2015)
17. F. Zanlungo, T. Ikeda, and T. Kanda, Social force model with explicit collision prediction, *Europhys. Lett.* 93(6), 68005 (2011)
18. G. Flötteröd and G. Lämmel, Bidirectional pedestrian fundamental diagram, *Trans. Res. Part B* 71, 194 (2015)
19. T. Xiong, P. Zhang, S. C. Wong, C. W. Shu, and M. P. Zhang, A macroscopic approach to the lane formation phenomenon in pedestrian counterflow, *Chin. Phys. Lett.* 28(10), 108901 (2011)
20. Y. Q. Jiang, S. C. Wong, P. Zhang, R. X. Liu, Y. L. Duan, and K. Choi, Numerical simulation of a continuum model for bi-directional pedestrian flow, *Appl. Math. Comput.* 218, 6135 (2012)
21. S. P. Hoogendoorn, F. L. M. van Wageningen-Kessels, W. Daamen, and D. C. Duives, Continuum modelling of pedestrian flows: From microscopic principles to self-organised macroscopic phenomena, *Physica A* 416, 684 (2014)

22. Y. Q. Jiang, S. G. Zhou, and F. B. Tian, A higher-order macroscopic model for bi-direction pedestrian flow, *Physica A* 425, 69 (2015)
23. Y. Q. Jiang, S. G. Zhou, and F. B. Tian, Macroscopic pedestrian flow model with degrading spatial information, *J. Comput. Sci.* 10, 36 (2015)
24. N. Bellomo and C. Dogbé, On the modeling of traffic and crowds: A survey of models, speculations, and perspectives, *SIAM Rev.* 53(3), 409 (2011)
25. N. Bellomo and L. Gibelli, Toward a mathematical theory of behavioral social dynamics for pedestrian crowds, *Math. Models Methods Appl. Sci.* 25(13), 2417 (2015)
26. D. Helbing, I. Farkas, and T. Vicsek, Simulating dynamical features of escape panic, *Nature* 407(6803), 487 (2000)
27. X. X. Yang, W. Daamen, S. P. Hoogendoorn, Y. Chen, and H. R. Dong, Breakdown phenomenon study in the bidirectional pedestrian flow, *Transpor. Res. Proc.* 2, 456 (2014)
28. R. Y. Guo, Simulation of spatial and temporal separation of pedestrian counter flow through a bottleneck, *Physica A* 415, 428 (2014)
29. L. Hou, J. G. Liu, X. Pan, and B. H. Wang, A social force evacuation model with the leadership effect, *Physica A* 400, 93 (2014)
30. T. Korecki, D. Palka, and J. Was, Adaptation of social force model for simulation of downhill skiing, *J. Comput. Sci.* 16, 29 (2016)
31. W. G. Weng, T. Chen, H. Y. Yuan, and W. C. Fan, Cellular automaton simulation of pedestrian counter flow with different walk velocities, *Phys. Rev. E* 74(3), 036102 (2006)
32. X. X. Jian, S. C. Wong, P. Zhang, K. Choi, H. Li, and X. N. Zhang, Perceived cost potential field cellular automata model with an aggregated force field for pedestrian dynamics, *Trans. Res. Part C.* 42, 200 (2014)
33. Y. Tajima, K. Takimoto, and T. Nagatani, Pattern formation and jamming transition in pedestrian counter flow, *Physica A* 313(3–4), 709 (2002)
34. R. Nagai and T. Nagatani, Jamming transition in counter flow of slender particles on square lattice, *Physica A* 366, 503 (2006)
35. L. B. Fu, W. G. Song, W. Lv, X. D. Liu, and S. M. Lo, Multi-grid simulation of counter flow pedestrian dynamics with emotion propagation, *Simul. Model. Pract. Theory* 60, 1 (2016)
36. D. R. Parisi and C. O. Dorso, Morphological and dynamical aspects of the room evacuation process, *Physica A* 385(1), 343 (2007)
37. D. R. Parisi, M. Gilman, and H. Moldovan, A modification of the social force model can reproduce experimental data of pedestrian flows in normal conditions, *Physica A* 388(17), 3600 (2009)
38. J. Kwak, H. H. Jo, T. Luttinen, and I. Kosonen, Collective dynamics of pedestrians interacting with attractions, *Phys. Rev. E* 88(6), 062810 (2013)
39. T. Kretz, A. Grosse, S. Hengst, L. Kautzsch, A. Pohlmann, and P. Vortisch, Quickest paths in simulations of pedestrians, *Advances in Complex Systems* 14(5), 733 (2011)
40. I. Karamouzas, B. Skinner, and S. J. Guy, Universal power law governing pedestrian interactions, *Phys. Rev. Lett.* 113(23), 238701 (2014)
41. J. Wahle, A. L. C. Bazzan, F. Klügl, and M. Schreckenberg, Decision dynamics in a traffic scenario, *Physica A* 287(3–4), 669 (2000)
42. W. X. Wang, B. H. Wang, W. C. Zheng, C. Y. Yin, and T. Zhou, Advanced information feedback in intelligent traffic systems, *Phys. Rev. E* 72(6), 066702 (2005)
43. B. K. Chen, X. Y. Sun, H. Wei, C. F. Dong, and B. H. Wang, Piecewise function feedback strategy in intelligent traffic systems with a speed limit bottleneck, *Int. J. Mod. Phys. C* 22(08), 849 (2011)
44. B. K. Chen, C. F. Dong, Y. K. Liu, W. Tong, W. Y. Zhang, J. Liu, and B. H. Wang, Real-time information feedback based on a sharp decay weighted function, *Comput. Phys. Commun.* 183(10), 2081 (2012)
45. B. K. Chen, W. Tong, W. Y. Zhang, X. Y. Sun, and B. H. Wang, Flux information feedback strategy in intelligent traffic systems, *Europhys. Lett.* 97(1), 14001 (2012)
46. B. K. Chen, Y. B. Xie, W. Tong, C. F. Dong, D. M. Shi, and B. H. Wang, A comprehensive study of advanced information feedbacks in real-time intelligent traffic systems, *Physica A* 391(8), 2730 (2012)
47. B. K. Chen, D. Z. W. Wang, Y. C. Gao, K. Zhang, L. X. Miao, and B. H. Wang, Effects of traffic lights for Manhattan-like urban traffic network in intelligent transportation systems, *Transportmetrica B*,
48. Y. T. Zhang, H. K. Zhao, and J. Qian, High order fast sweeping methods for static Hamilton Jacobi equations, *J. Sci. Comput.* 29(1), 25 (2006)